Metallo-responsive self-assembly of lipophilic guanines in hydrocarbon solvents: a systematic SAXS structural characterization

Metallo-responsive self-assembly of lipophilic guanines in hydrocarbon solvents: a systematic SAXS structural characterization.†

Adriano Gonnelli,[a] Silvia Pieraccini,[b] Enrico J. Baldassarri,[a;c] Sergio Funari,[d] Stefano Masiero,[b;*] Maria Grazia Ortore[a] and Paolo Mariani[a;*]

[a]Dipartimento di Scienze della Vita e dell'Ambiente, Biophysics Research Group, Università Politecnica delle Marche, Via Brecce Bianche, 60131Ancona, Italy. E-mail: p.mariani@univpm.it

[b]Dipartimento di Chimica "G. Ciamician", Università di Bologna, Italy. E-mail: stefano.masiero@unibo.it

[c]Marche Structural Biology Center, Università Politecnica delle Marche, Via Brecce Bianche, 60131 Ancona, Italy.

[d]HASYLAB, Hamburg, Germany.

Lipophilic guanines (LipoGs) in aprotic solvents undergo different self-assembly processes based on different H-bonded motifs. Cylindrical nanotubes made by p-pstacked guanine tetramers (G-quadruplexes) and flat tape-like aggregates (G-ribbons) have been observed depending on the presence of alkali metal ions. To derive information on the structural properties and stability of these LipoG aggregates, Small-Angle X-ray Scattering (SAXS) experiments have been performed in dodecane, both in the presence and in the absence of potassium ions. As a result, the occurrence of the two different metallo-responsive architectures (nanoribbons or columnar nanotubes) was confimed and we reported here for the firs time a systematic study on the dependence of the aggregate properties on composition, temperature and molecular units structure. Even if dodecane was selected to favour LipoG solubility, a strong tendency to self-organization into ordered lyotropic phases was indeed detected.

Introduction

It is well known that organic nanoarchitectures (as nanotubes and nanowires) form in solution by self-assembly of molecular and supramolecular motifs, such as cyclic peptides, dendrimers, DNA and surfactants[1–8]. In all cases, and unlike inorganic nanotubes, the formed nanostructures are dynamic systems stabilized by inter and intra-molecular interactions and by solvophobic effects. This special characteristic allows modular self-assembly with a rich structural diversity, through a delicate balance between different interactions, thanks to a proper choice of experimental conditions and a fine control of the properties of the building blocks by functional synthesis (see, e.g.,[9,10]).

Among the different self-assembling motifs, guanine (G) is a singular system, possessing a polarized aromatic surface coupled with different donor (N^1H and N^2H) and acceptor sites (O^6, N^3 and N^7), located in a self-complementary arrangement. In water, guanine shows self-assembling, with the formation of G-quartets by multiple hydrogen bonding of four G in the so-called Hoogsteen mode, and π-π stacking, with the formation of long, helical aggregates named G-quadruplexes, as shown for guanosine 5'-monophosphate (GMP) in Fig. 1. Being appropriately sized to fit into the cavity located between two G-quartets and because of interactions with the O^6 carbonyl groups of the eight guanines, metal ions have been observed to enhance base-stacking forces, thus controlling length and thermal stability of G-quadruplexes[11–22].

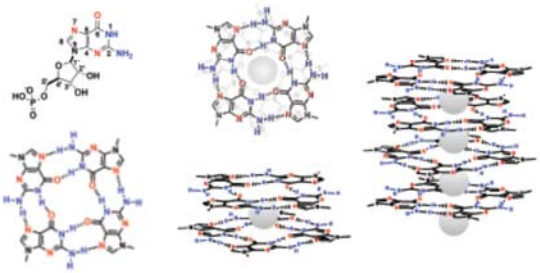

Fig. 1 Representation of the aggregates formed by GMP in water. From the left: G-quartet, G-octamer (dimer of G-quartets), G-quadruplex. In the GMP molecule, the H-donor and acceptor sites are highlighted.

Lipophilic guan(os)ines (LipoGs), *i.e.*, G-derivatives with different lipophilic substituents attached to the sugar moiety or directly replacing the sugar unit, show similar but more heterogeneous supramolecular properties when dissolved in organic solvents [23–28]. Indeed, evidences for the formation of at least two different architectures based on different, self-complementary hydrogen bond schemes were reported. In the first case, LipoG/metal

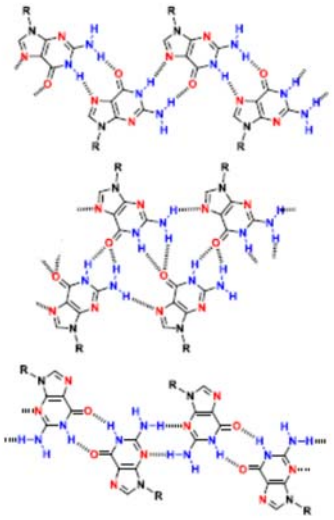

Fig. 2 Ribbon-like assemblies of LipoG derivatives, as observed in organic solvents in the absence of salt.

ion complexes were obtained by addition of potassium picrate (KPi): NMR and CD data suggested the formation of G-octamers and pseudo-polymeric G-quadruplexes[29,30], that X-ray diffraction experiments in condensed phases confirmed to be formed by stacked G-quartets, with cations sandwiched in between adjacent quartets[31]. Conversely, by dissolving LipoGs in chloroform solution in the absence of salts, the formation of largely self-associated ribbon-like structures was observed on flat surfaces by STM and in the solid state by NMR[32]. Moreover, new 2D lyotropic mesophases made of supramolecular nanoribbons were evidenced by X-ray diffraction[33–35] (see Fig. 2). Therefore, it was assessed that for guanosine derivatives (without sterically demanding groups on the guanine base) the formation of supramolecular nanoribbons in solution, in the solid state, and on flat surfaces is universal.

LipoG architectures have attracted much interest for possible (bio)technological applications at the nanometric and micrometric scales. Indeed, G-quartets were used as ion channels for transport through a phospholipid membrane[36] or as sensors anchored at Langmuir monolayers or living cell membranes[37], while G-nanoribbons were proposed for constructing molecular electronic nanodevices[38]. In addition, based on either G-quartets or ribbon-like H-bonded networks, different nanomaterials were fabricated, like reversible organogels with photoconductive properties[39], hy-

brid organic-inorganic systems for conduction and optical applications[40,41], flexible and self-supporting films[42], functional microporous films or membranes,[43,44] and nano- and microcapsules with high stability in highly polar aqueous media[45]. In this context, new insights into structural features and dynamics of LipoG arrangements in solution, as well as relationship between the molecular level and the supramolecular organization, represent a key step for designing new materials with specific properties and functions. While the G-quartet structure is the one normally observed in water, the ribbon structure exists exclusively in the case of lipophilic derivatives in apolar media or in the solid state, and it is stable upon drying/dissolution. This paves the way to possible applications of this architecture in lipidic environments (mimicked here by the hydrocarbon solvent, see e.g.[37]) where, analogously to nucleolipids[46], should likely pose no biocompatibility issues.

LipoG quadruplexes formed in diluted conditions in cyclohexane and in the presence of K, Na and Sr picrate and KI were recently investigated by Small-Angle X-ray Scattering (SAXS)[47]. As a main result, the structural features of octamers and pseudo polymeric G-quadruplexes and their amount at the equilibrium were obtained. However, no data were collected on ribbon-like assemblies. Since a fine SAXS characterisation of these superstructures was lacking, similar experiments have been now performed on LipoGs dissolved in dodecane, at very low concentrations and both in the absence and in the presence of potassium picrate (KPi). Dodecane was used as solvent, because of its high boiling point, the rather large solubility of the different investigated compounds and the already detected ability to promote solute-solute intermolecular H-bonds[33]. To confirm the influence of salt on self-assembling, but mainly to derive information on elongation, flexibility and thermal stability of the different architectures, SAXS data were analysed considering different possible structural motifs and using a global data fitting approach. While the presence of the two expected supramolecular architectures was confirmed, a strong tendency of both nanoribbons and G-quadruplexes to interact and to phase-separate in ordered lyotropic phases has been also detected.

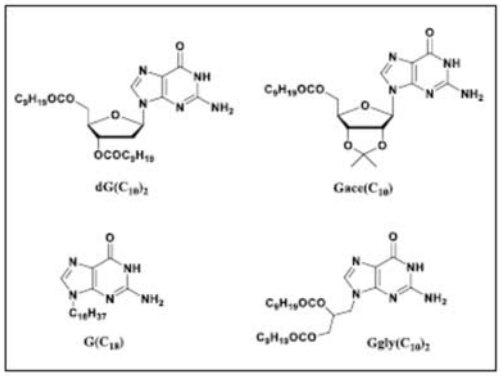

Fig. 3 Molecular formula of the different investigated LipoGs

2 Materials and methods

2.1 Materials and procedures

The four LipoGs considered, synthesized as previously reported[25,47,48], are shown in Figure 3. For preparing samples in the presence of KPi, 8 mg of each LipoG were added with *ca.* 4 mg of KPi and 0.8 mL of chloroform (typically used for promoting ion-templated complexation of LipoG derivatives) in a 4ml glass vial (15 mm in diameter). The suspensions were stirred for three days at room temperature, then the excess of solid salt was removed by centrifugation. For each derivative, 0.6 mL of the clear chloroform solution containing the LipoG/KPi complex were dried at *ca.* 40°C for 12 hours and added with 0.6 mL of dodecane to obtain the 1.3% wt sample. The 0.26% wt dodecane solutions were obtained by further five time dilution. Samples in the absence of KPi (1.2 wt%) were prepared by dissolving *ca.* 7 mg of the requested LipoG into 0.8 mL of dodecane, by heating when necessary. All prepared samples were stored at room temperature and appeared as stable solutions for at least 10 days.

The studied conditions are listed in Table 1.

Table 1 Investigated LipoG samples and conditions.

LipoG	salt	*c* (wt%)	*T* range (°C)
$dG(C_{10})_2$	no	1.2	20 ÷ 90
$dG(C_{10})_2$	KPi	0.26 / 1.3	25 ÷ 95
$Gace(C_{10})$	no	1.2	20 ÷ 90
$Gace(C_{10})$	KPi	0.26 / 1.3	25 ÷ 95
$Ggly(C_{10})_2$	no	1.2	20 ÷ 90
$Ggly(C_{10})_2$	KPi	0.26 / 1.3	25 ÷ 95
$G(C_{18})$	no	1.2	20 ÷ 90
$G(C_{18})$	KPi	0.26 / 1.3	25 ÷ 95

2.2 SAXS experiments

SAXS experiments were performed at the DESY synchrotron (Hamburg, Germany) at the A2 beam-line, during 2 different beam-time allocations. The investigated Q-range ($Q=4\pi \sin\theta/\lambda$, where 2θ is the scattering angle and $\lambda=1.50$ Å the X-ray wavelength) was 0.026-0.33 $Å^{-1}$ in the first and 0.02-0.23 $Å^{-1}$ in the second beam-time allocation. 1 mm diameter quartz capillaries were used. Scattering data were recorded on a bi-dimensional MAR CCD 126 detector with 1024x1024 pixels, radially averaged and corrected for the dark, detector efficiency, sample transmission and solvent contribution, as usual[49]. No absolute scale calibration of the experimental data was available.

Experiments were run at different temperatures, as indicated in Table 1. Particular attention was paid to check for equilibrium conditions and to monitor radiation damage. In a few tests, measurements were repeated several times (up to 30) at the same temperature or on refilled capillaries to account for a constant scattering signal. Accordingly, to avoid radiation damage the exposure time was 180 s/frame, while to establish equilibrium condition during heating cycles the dead-time was around 5 minutes.

2.3 SAXS data analysis and fitting

The SAXS curves here obtained (see Figures 4 and 5) are usually featureless, but in a few conditions Bragg peaks, or at least a large band dominating the low-angle scattering, were detected (see, e.g., $dG(C_{10})_2$ in the presence and in the absence of KPi, respectively). Therefore, the data analysis was differently managed.

In the presence of Bragg peaks, the analysis was limited to the determination of the peak position. Because in all the different cases only one peak was observed, peak indexing was not possible and then the structure of the lyotropic phase was described considering previous results obtained at higher concentrations.

In the absence of Bragg peaks, SAXS curves were investigated by standard Guinier's analysis[50] and by using a global fitting approach[51]. At one side, a linearized representation of the X-ray scattering intensity $I(Q)$ in term of $\ln(I(Q))$ vs Q^2 or $\ln(I(Q)Q)$ vs Q^2) plots allows the determination of the particle gyration radius (R_g, related to the average particle size) or of the radius of gyration of the particle cross-section (R_c, related to the size of the particle section)[52,53]. At the other side, a global fitting analysis, based on the simultaneous fit of several scattering curves using singular and common set of parameters, allows to obtain unambiguous information on particle shape, size and size-distribution, overcoming effects due to model parameter correlations and unreliability.

The model fitting procedure is here shortly described. The excess X-ray scattering intensity $I(Q)$ can be written as[50]:

$$I(Q) = \kappa N_p P(Q) S_{meas}(Q) \tag{1}$$

where N_p is the number density of the scattering particles, κ a calibration factor (which is related to the absolute units of the scattering cross section) and $P(Q)$ and $S_{meas}(Q)$ are the particle effective form factor and the measured structure factor, respectively.

$S_{meas}(Q)$ is related to particle-particle interactions, which are usually negligible in dilute solutions ($S_{meas}(Q) \approx 1$). However, both nanoribbons and G-quadruplexes in dodecane show a strong tendency to interact: van der Waals attraction (which could be responsible for the phase-separation detected for example in $dG(C_{10})_2$/KPi or in $Ggly(C_{10})_2$ samples) and short-range steric repulsion (which contributes for example to the swelling behaviour observed in $Gace(C_{10})$/KPi at 1.3 wt%, see below Table 2) could balance in a few cases, and modulate interactions that eventually manifest even at these low concentrations as a low-intensity band in the scattering profile. The evaluation of the $S_{meas}(Q)$ has been performed considering the basic and simple approximation of a two-body hard-sphere interaction potential[54], which has been already demonstrated to be very convenient for a coarse estimate of particle-particle interactions in similar systems[47]. References[49] and[55] provide complete details on the potential and the form factor, whose fitting parameters are the effective particle diameter, σ_{eff}, and the excluded volume, ϕ_{sphere}.

The effective form factor $P(Q)$ was derived using different simple models based on the expected self-assembling patterns. For the G-quadruplex, $P(Q)$ was described considering straight cylinders with circular section of radius R and composite scattering length density profile (see[47,54]). Because dodecane and guanine hydrocarbon chains show the same electron density (ρ_{solv}=ρ_{chain}=0.26 $e^-/Å^3$), the cylinder cross-section was split into only two homogeneous regions: an inner cavity (radius r_{core} and electron density ρ_{core}), where cations are expected to be located, and a shell of thickness ($R - r_{core}$) and electron density ρ_{sh}, which corresponds to the guanine (and sugar) regions[47,53]. According to possible elongation mechanisms[47], a polydispersity of the cylinder length H was included by integrating the orientationally averaged form factor of the cylinder over a Schulz distribution of its length[56,57]. In particular:

$$P(Q) = \kappa \int_0^x f(H)dl \int_0^{\pi/2} F^2(Q,\alpha)\sin(\alpha)d\alpha \tag{2}$$

where $f(H)$ is the normalized Schulz distribution of the length (note that $x = H/H_{avg}$, being H_{avg} the mean cylinder length) and $F(Q,\alpha)$ is the core-shell cylinder form factor:

$$F(Q,\alpha) = 2(\rho_{core} - \rho_{sh})\pi r_{core}^2 H \frac{\sin(QH\cos\alpha)}{QH\cos\alpha} \frac{J_1(Qr_{core}\sin\alpha)}{Qr_{core}\sin\alpha} + 2(\rho_{sh} - \rho_{solv})\pi R^2 H \frac{\sin(QH\cos\alpha)}{QH\cos\alpha} \frac{J_1(QR\sin\alpha)}{QR\sin\alpha}$$

The fitting parameters were the radii and electron densities of the cylinder and the mean value and variance of the G-quadruplex length distribution.

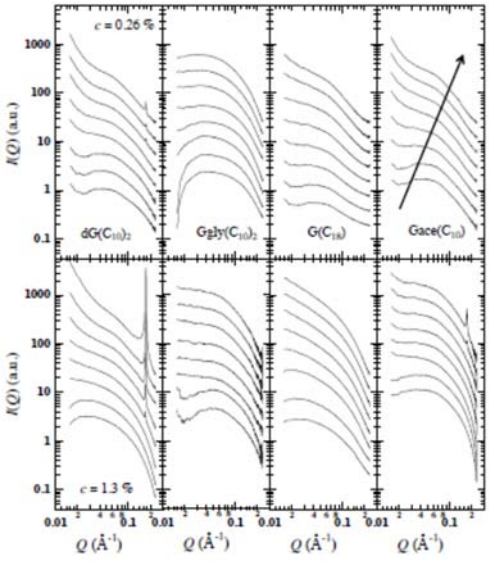

Fig. 4 Log-log SAXS profiles observed from LipoGs in dodecane in the presence of KPi at different temperatures. The LipoG concentration was c=0.26 wt% (curves in the top row) and c=1.3 wt% (curves in the bottom row). Curves are scaled for clarity: as an indication, the arrow in the top, right frame points out the temperature change, from 25° to 95°C (with 10° steps).

For the ribbon-like aggregates, the form factor was calculated

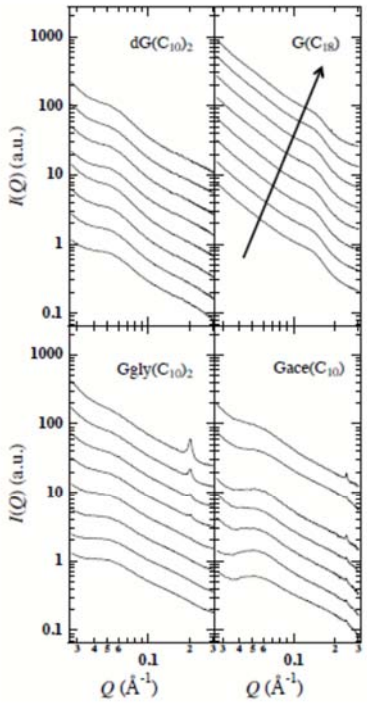

Fig. 5 Log-log SAXS profiles observed from LipoGs in dodecane in the absence of KPi at different temperatures. The LipoG concentration was c = 1.2 wt%. Curves are scaled for clarity: as an indication, the arrow in the top, right frame indicates the temperature change from 20° to 90°C (with 10° steps).

considering a worm-like model, based on a flexible rod with elliptical cross section (which excludes the guanine hydrocarbon chains) and a uniform scattering length density[58]. In the model, the flexible rod of total length C_l (the contour length) is described by a number of locally stiff segments of length l_p (the persistence length, the length along the chain over which the flexible rod can be considered rigid). The non-negligible cross section of the rod is included by accounting for excluded volume interactions within the walk of a single segment. Then, the fitting parameters were the contour length C_l, the Kuhn length (*i.e.*, $2l_p$) and the chain cross-section semi-axes $A/2$ and $B/2$[58].

3 RESULTS AND DISCUSSION

SAXS results obtained from LipoG samples prepared in dodecane (0.26 to 1.3 wt%) in the presence and in the absence of KPi, are shown in Figures 4 and 5, respectively. Data show that the overall scattering profile is influenced by the presence of the salt, suggesting that addition of potassium ions is responsible for the formation of different aggregate species in solution. Moreover, the scattering intensity changes on heating, indicating that stability of aggregates is controlled by temperature.

The occurrence of a large band dominating the low-angle region (see, e.g., the Gace(C_{10})/KPi sample at c=0.26 wt% in Fig.5 or the dG(C_{10})$_2$ sample at c=1.2 wt% in Fig.4) or even the presence of Bragg peaks (see, e.g., the dG(C_{10})$_2$/KPi sample at both the analysed concentrations in Fig. 5 or the Ggly(C_{10})$_2$ sample at c=1.2 wt% in Fig.4) are really surprising at the relatively low concentrations here investigated. Indeed, they are clear indications of the presence of strongly correlated system and eventually of the formation of ordered phases. Featureless curves were indeed detected for analogous samples dissolved in cyclohexane at similar concentrations[47], proving that the solvent plays a crucial role in the early formation of supramolecular assemblies.

The general behaviour is summarised in Table 2: it has to be noticed that in the presence of Bragg peaks the profile features have been labeled according to the structure of the proximate lyomesophase, already characterised in more concentrated conditions[31,59].

Table 2 Summary of the results. SAXS curve features are indicated as "diffuse" if a large and diffuse band is present, "BP" if Bragg peaks are present, "band" if a high intensity diffuse peak is present; the phase assignment is the following: *I* for isotropic liquid phase, *H* and *R* for hexagonal or rectangular columnar phases, *N* for nematic phase. *a* is the unit cell parameter, as derived from the position of the Bragg peak according to the assigned structure; T_m is the *H-I* phase-transition temperature. *a* and T_m ranges are eventually reported if a concentration dependence is observed.

sample	*features*	*a* (Å)	*phase*	T_m (°C)
dG(C_{10})$_2$	diffuse	-	*I*	-
dG(C_{10})$_2$/KPi	BP	36.3-36.1	*H*	50-70
Gace(C_{10})	band/BP	≃120/25.6	*N*/*R*	-
Gace(C_{10})/KPi	BP	47.6-36.4	*H*	45-85
Ggly(C_{10})$_2$	BP	30.9	*H*	45
Ggly(C_{10})$_2$/KPi	-	-	*I*	-
G(C_{18})	diffuse	-	*I*	-
G(C_{18})/KPi	-	-	*I*	-

3.1 Structure of the supramolecular assemblies

Guinier analysis of SAXS profiles provided the first information on LipoG self-assembled architectures. In particular, Guinier plots for rod-like particles ($\ln(I(Q)Q)$ vs Q^2) allowed to confirm the presence of elongated supramolecular objects and to obtain the radius of gyration of their cross-section, R_c. A few representative examples are reported in Figure 6 (note that in the presence of correlation bands, such an analysis was not possible).

The whole cross-sectional radii analysis is resumed in Figure 7. In the presence of KPi, the cross-sectional radii of gyration, R_c, show a minor reduction with temperature, but a clear independency on the considered LipoG derivative and on its concentration. R_cc, centred around 8 Å, are in very good agreement with the radii estimated from G-quadruplex molecular models (the calculated R_c value of the tetrameric core is around 8.5-7 Å, depending on whether the sugar residues are considered or not). Samples dissolved in dodecane in the absence of KPi show lower R_c values, centered around 4 Å, irrespective of temperature and na-

Table 3 Single and common parameters obtained by the global-fitting procedure applied to G(C_{18}) SAXS data. Errors in cylinder length and in the ribbon contour and Kuhn lengths are around 10%; errors in electron densities are $\pm$ 0.02 $e^-/Å^3$; errors in σ_{eff} and ϕ_{sphere} are around 4%. Symbols as in the text.

G(C_{18})/KPi, c=1.3 wt%							**G(C_{18})**, c=1.2 wt%						
cylinder model							**ribbon model**						
T (°C)	25	35	45	55	65	75	T (°C)	20	30	40	50	60	70
length (Å)	248	214	185	130	103	85	contour l. (Å)	807	765	723	720	710	650
polydisp.	0.27	0.39	0.49	0.56	0.50	0.39	Kuhn l. (Å)	60.0	53.9	58.2	63.0	57.9	60.7
ρ_{core} ($e^-/Å^3$)	0.38	0.37	0.38	0.36	0.35	0.37	σ_{eff} (Å)	20.7	21.2	21.2	21.4	21.6	21.5
							ϕ_{sphere}	0.06	0.08	0.08	0.08	0.09	0.08
ρ_{sh} ($e^-/Å^3$)	0.47						ρ_{rbn} ($e^-/Å^3$)	0.47					
R (Å)	13.7 $\pm$ 0.8						$A/2$ (Å)	3.2 $\pm$ 0.4					
r_{core} (Å)	1.3 $\pm$ 0.3						axis ratio	3.7 $\pm$ 0.5					

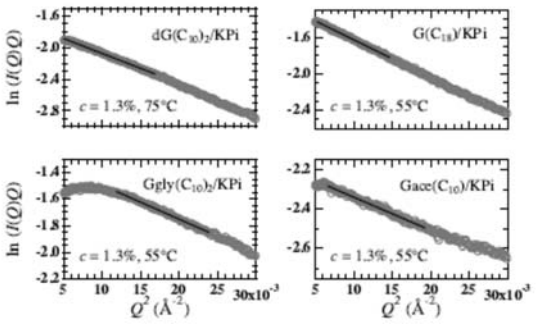

Fig. 6 Elongated rod-particles Guinier analysis of SAXS curves for LipoGs dissolved in dodecane, in the presence of KPi. Concentration and temperatures are indicated in the different frames. Continuous lines are the Guiner best fits.

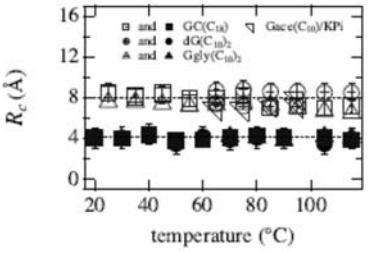

Fig. 7 Temperature dependence of the particle cross-sectional radii of gyration, R_c, as derived in the presence (open symbols) and absence (filled symbols) of KPi.

ture of the LipoG derivative. This lower dimension agrees with the presence of ribbon-like superstructures, like those depicted in Figure 2 (the averaged cross-sectional radius of gyration of a ribbon, estimated from molecular models, is about 4.3 Å).

3.2 Model fitting: the case of G(C_{18})

Model data fitting was performed on high concentrated samples to derive particles shape and size. Here, results obtained in the special case of the G(C_{18}) compound will be detailed.

According to Guinier results described above, G(C_{18}) data were analysed considering the possible presence of pseudo-polymeric LipoG-quadruplexes or nanoribbons. As a clear outcome, SAXS data obtained in the presence of KPi were best fitted by using the effective form factor for circular cylinders with a core-shell scattering length density profile and polydisperse height (see[54] and Eq.2). Best fitting curves are superposed to experimental data in Figure 8, and the very consistency of the model is evident. The relevant fitting parameters are reported in Table 3 and in Figure 9. Structural data (*i.e.*, radii and electron densities) appear fully consistent with the presence of G-quadruplexes, made of *ca.* 70 piled G-quartets at 25°C. The G-quadruplex gradually disassem-

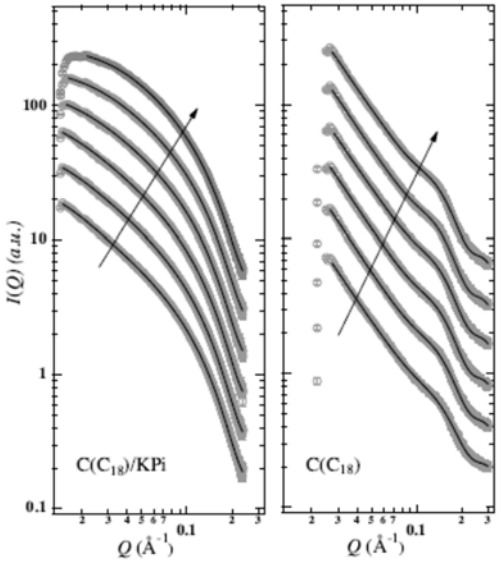

Fig. 8 SAXS profiles observed for G(C_{18}) in the presence and absence of KPi at different temperatures. Curves are scaled for clarity. Left side, c=1.3 wt% with KPi and temperatures from 25° to 75°C with 10° steps, as indicated by the arrow; right side: c=1.2 wt% and temperatures from 20° to 70°C with 10° steps, as indicated by the arrow. Continuous lines are best fit curves; the fitted Q-range corresponds to the length of the traced lines.

bles on heating: as shown in Fig. 9, the variance of the quadruplex length distribution is larger when particles are longer (*i.e.*, at low temperatures), as expected for an isodesmic elongation mechanism.[47] Another point should be underlined: the rather constant electron density of the G-quartet core (ρ_{core}) is a strong indication of the fact that the inner cavity of the quadruplexes is filled by cations. As previously observed in cyclohexane[47], the hole potassium occupancy, calculated as the ratio $\rho_{core}V_{core}/N_K$, where V_{core} is the volume of the inner cavity and N_K is the number of electrons for the potassium ion, resulted around 75% at all the investigated temperatures.

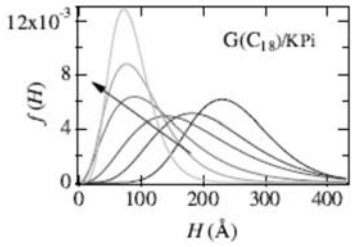

Fig. 9 Temperature dependence of the length polydispersity of the model cylinder used to fit G(C_{18})/KPi SAXS data (c = 1.3 wt%). The arrow points out the temperature change from 25° to 75°C (with 10° steps).

SAXS data obtained with G(C_{18}) solutions prepared in the absence of KPi are very different (compare profiles in Fig. 8). In particular, a characteristic broad band at $Q_{max} = 0.15$ Å^{-1}, which indicates interaction among structure elements, is detected. Model fittings show that the form factor of a worm-like flexible particle with elliptical cross section and uniform scattering length density, combined with a spherically symmetric two-body hard-sphere interacting potential, best reproduces the data. Best fitting curves are shown in Figures 8 and 10 (where the different $P(Q)$ and $S(Q)$ contributes at 60°C are reported separately), while fitting parameters are listed in Table 3. Three points should be underlined. *First*, the broad band which characterizes the SAXS curves is very well reproduced by using a rather smooth hard-sphere potential (see Figure 8), suggesting that only minor, repulsive short-range particle-particle interactions occur in this system. Indeed, a small increase in ϕ_{sphere} is detected as a function of temperature. At the same time, the structure factor at Q=0 meaningfully decreases at increasing temperature, while its first peak intensity adequately increases, as clearly shown in the right panel of Fig. 10. Both these results are congruent with an increase of the number of interacting particles in solution, possibly determined by ribbon disassembly on heating. *Second*, the fitted electron density, ρ_{rbn}, and the size of the particle section ($S^* = \pi AB/4 = 128 \pm 23$ Å^2) are in full agreement with what expected for a single ribbon: in particular, the guanosine ribbon I cross-section determined from molecular models is around 110 Å^2 [60]. *Third*, the aggregates are long, but relatively flexible, being the number of statistical segments in the range from 13 to 10 when the temperature increases from 20 to 70°C. Interesting is the fact that the persistence length (l_p, half of the Kuhn length) is constant, and corresponds to about twice the length of the guanine repeat unit along the ribbon. On the other side, the small decrease of the ribbon contour length as a function of temperature, even inside the experimental errors, seems to confirm the suggested ribbon disassembling.

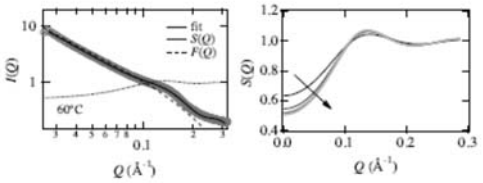

Fig. 10 Fitting results for G(C_{18}) in dodecane (c = 1.2 wt%). Left side: fitting analysis of the SAXS curve measured at 60°C: the $P(Q)$ and $S(Q)$ contributions are shown separately (see Eq.1). Right side: $S(Q)$ structure factors as derived as a function of temperature by fitting procedure. The arrow points out the temperature change from 25° to 75°C (with 10° steps).

3.3 Model fitting: the other LipoGs

When applicable, model data fitting was also performed to SAXS curves related to the other investigated LipoGs. Best fitting parameters are reported in Table 4.

G-quadruplex formation in the presence of KPi is confirmed for all derivatives (see Table 4, cylinder model). Interestingly, quadruplexes are particularly short (*i.e.*, made by less than 15-20 piled G-quartets), with a very low length polydispersity for the Ggly(C_{10})$_2$ and Gace(C_{10}) cases. Electron density values indicate that quadruplex central cavity is filled by potassium ions, although the corresponding average cation hole occupancy factor is around 75% for Ggly(C_{10})$_2$ and dG(C_{10})$_2$, but lower than 60% for Gace(C_{10}) (note that because the intrinsically low experimental resolution, errors in electron density determination and then in occupancy factor calculations are large, and a more precise detail on fitted numbers is definitely unphysical).

In the absence of salt, model fitting confirms the formation of elongated flat particles, with an elliptical cross-section of area fully consistent with the hydrogen-bonding guanine ribbon-like motifs. In the case of Ggly(C_{10})$_2$, ribbons are *infinitely* long and rather rigid, while they are flexible and with a contour length very dependent on temperature in the case of dG(C_{10})$_2$. The markedly different flexibility could be indicative of different self-assembly patterns: as the ribbon I structure can be assigned to dG(C_{10})$_2$ on the basis of previous experiment in solution and at the solid-liquid interface,[61] a different ribbon arrangement with a stronger H-bond network may occur for Ggly(C_{10})$_2$ (see e.g. the different hydrogen-bonding motifs that characterize the "narrow" and the "wide" ribbon structures for dG(C_{10})$_2$ itself in the solid state[35]).

Table 4 Single and common parameters obtained by the global-fitting procedure applied to analyzable SAXS data. Errors in cylinder length and in the ribbon contour and Kuhn lengths are around 10%; errors in electron densities are $\pm 0.02\ e^-/\text{Å}^3$; errors in σ_{eff} and ϕ_{sphere} are around 5%. Symbols as in the text, but ∞ means "longer than 2000 Å" and - "data fitting not appropriate".

Ggly(C_{10})$_2$/KPi, c=1.3 wt%

cylinder model						
T (°C)	25	35	45	55	65	75
length (Å)	58	59	56	47	43	40
polydisp.	0.10	0.11	0.13	0.11	0.24	0.26
ρ_{core} ($e^-/\text{Å}^3$)	0.39	0.39	0.38	0.38	0.38	0.37
ρ_{sh} ($e^-/\text{Å}^3$)	0.47					
R (Å)	12.4 ± 0.5					
r_{core} (Å)	1.2 ± 0.2					

Ggly(C_{10})$_2$, c=1.2 wt%

ribbon model						
T (°C)	20	30	40	50	60	70
contour l. (Å)	-	-	-	-	∞	∞
Kuhn l. (Å)	-	-	-	-	164	159
σ_{eff} (Å)	-	-	-	-	48.3	48.6
ϕ_{sphere}	-	-	-	-	0.08	0.09
ρ_{rbn} ($e^-/\text{Å}^3$)	0.47					
$A/2$ (Å)	3.4 ± 0.8					
axis ratio	3.7 ± 0.7					

Gace(C_{10})/KPi, c=1.3 wt%

cylinder model						
T (°C)	25	35	45	55	65	75
length (Å)	-	-	54	52	52	54
polydisp.	-	-	0.13	0.11	0.12	0.14
ρ_{core} ($e^-/\text{Å}^3$)	-	-	0.32	0.31	0.32	0.30
ρ_{sh} ($e^-/\text{Å}^3$)	0.47					
R (Å)	12.3 ± 0.8					
r_{core} (Å)	1.3 ± 0.5					

Gace(C_{10}), c=1.2 wt%

ribbon model						
T (°C)	20	30	40	50	60	70
contour l. (Å)	-	-	-	-	-	-
Kuhn l. (Å)	-	-	-	-	-	-
σ_{eff} (Å)	-	-	-	-	-	-
ϕ_{sphere}	-	-	-	-	-	-
ρ_{rbn} ($e^-/\text{Å}^3$)	-					
$A/2$ (Å)	-					
axis ratio	-					

dG(C_{10})$_2$/KPi, c=1.3 wt%

cylinder model						
T (°C)	25	35	45	55	65	75
length (Å)	-	-	-	-	-	64
polydisp.	-	-	-	-	-	0.28
ρ_{core} ($e^-/\text{Å}^3$)	-	-	-	-	-	0.37
ρ_{sh} ($e^-/\text{Å}^3$)	0.47					
R (Å)	12.9 ± 1.0					
r_{core} (Å)	1.4 ± 0.6					

dG(C_{10})$_2$, c=1.2 wt%

ribbon model						
T (°C)	20	30	40	50	60	70
contour l. (Å)	1200	850	490	540	530	495
Kuhn l. (Å)	18.4	16.5	16.0	15.9	16.1	16.1
σ_{eff} (Å)	46.9	46.7	45.1	45.6	44.9	45.0
ϕ_{sphere}	0.07	0.07	0.06	0.06	0.07	0.06
ρ_{rbn} ($e^-/\text{Å}^3$)	0.47					
$A/2$ (Å)	3.5 ± 0.4					
axis ratio	7.4 ± 0.3					

3.4 Ordered lyotropics and strongly correlated systems

As summarized in Table 2, Bragg peaks occur in some SAXS profiles, both in the presence (Figure 4) and in the absence of KPi (Figure 5). Because phase separation, results will be discussed only qualitatively, taking into account previously reported data.

dG(C_{10})$_2$: Concerning dG(C_{10})$_2$, the formation of ordered liquid-crystalline phases at low concentrations was already described: in the absence of salt, a 2D-square packing of ribbons were observed both in toluene (at 4%, w/w) and in hexadecane (at 8%, w/w) by X-ray diffraction[48], but in the presence of KPi, columnar cholesteric and hexagonal phases, based on G-quadruplexes, appeared to form in heptane at concentrations higher than 6% (w/w)[59].

In the present case, ~~mutual~~ interacting flexible nanoribbons were observed in the absence of KPi (Figure 5), while the SAXS profiles obtained in the presence of KPi are characterised by a Bragg peak at Q = 0.173 Å^{-1} (see Figure 4). Due to the experimental set-up, no other peaks were observed and the structure of the phase cannot be assigned. However, the peak position roughly corresponds to the position of the (1,0) peak of the hexagonal phase observed in heptane for the same LipoG at higher concentration and in the presence of the same salt[59]. Therefore, it can be argued that in dodecane the columnar hexagonal phase made by G-quadruplexes forms already at very low concentration. Noticeably, the peak position is slightly dependent on concentration, indicating a small, but general swelling behaviour: the 2D hexagonal unit cell increases from 41.7 to 41.9 Å when the concentration changes from 1.3 to 0.26 %). Upon heating, the peak reduces in intensity and finally vanishes at around 50°C at c=0.26 % and 70°C at c=1.3 %, indicating that a direct transition from the hexagonal to the isotropic phase occurs. Note that similar temperatures were detected in heptane and in the presence of KPi in correspondence of the cholesteric-to-isotropic phase transition and of the hexagonal-to-cholesteric phase transition[59] (Table 4).

Gace(C_{10}): Regarding Gace(C_{10}), while no mesogenic properties were reported in the presence of salts, a birefringent gel-like phase was described in toluene (or chloroform) without salts at c >2.5% (w/w)[62]. X-ray diffraction experiments performed at higher concentrations confirmed the existence of an ordered structure made by *infinitely* long nanoribbons, packed in a 2D-rectangular lattice (unit cell parameters were a=25.9 Å and b=10 Å at c=50%).

The Bragg peak observed in SAXS data obtained in the absence of KPi suggests that the same lyotropic ordered phase exists in dodecane. Indeed, its position ($2\pi/Q$= 25.6 Å) perfectly corresponds to the unit cell parameter a of the 2D-rectangular lattice previously determined. Due to the diluted conditions, the situation is however more complicated, as a wide band is further detected at Q=0.053 Å^{-1}. This band probably indicates the contemporaneous presence of a less ordered phase, possibly a nematic, formed by weak interacting ribbons. Interestingly, the band becomes better and better defined by increasing the temperature, even if the particle-particle correlation distance remains constant (about 120 Å), suggesting that the two phases are in equilibrium.

The formation of an ordered structure is also detected in the presence of KPi. A Bragg peak is indeed observed at large Q, in a position which depends on concentration. Assuming a possible 2D-hexagonal packing of G-quadruplexes, a swelling behaviour is detected: the unit cell increases from 42 to 55 Å when c decreases from 1.3 to 0.26 % w/w. It should be noticed that the peak disappears when the temperature exceeds 35°C, suggesting that a direct transition from the hexagonal to the isotropic phase occurs also for this LipoG (accordingly, fitting results in Table 4 indicate that quadruplexes are rather short[63]).

Ggly(C_{10})$_2$: For Ggly(C_{10})$_2$, gel- or liquid-crystalline phases have not been described before. The present SAXS data indicate that an ordered structure forms in dodecane in the absence of KPi. As only one Bragg peak at Q= 0.2 Å^{-1} is detected, the phase cannot be assigned. The peak disappears on heating at about 55°C, at a temperature in which a wide band dominates the low-angle region: a transition from a long-range ordered phase to a correlated organization of very long nanoribbons can be inferred.

4 CONCLUSION

Self-assembling properties of different LipoG derivatives dissolved in dodecane in dilute conditions have been investigated by SAXS. In all cases, the formation of supramolecular elongated, pseudo-polymeric aggregates, *i.e.*, quadruplexes or nanoribbons, has been demonstrated.

As expected[48,60,62], the formation of quadruplexes or nanoribbons is dictated by the presence or the absence of salt, although the structural properties of the supramolecular assemblies depend on the LipoG chemical structure. In all the considered cases, ribbons are very long, suggesting that their formation and elongation primarily depends on hydrogen donor-acceptor complementarity. However, different flexibilities emerge in different cases. In particular, ribbons made by dG(C_{10})$_2$ are very flexible, and show a persistence length of the order of the guanine repeat unit, while nanoribbons generated from G(C_{18}) and Ggly(C_{10})$_2$ show a persistence length from 2 to 6 times the guanine repeat unit, respectively, indicating less and less flexible objects. On the basis of previous data and according to the derived structural properties, nanoribbons of type I are suggested to form in dG(C_{10})$_2$ and G(C_{18}) dodecane solutions, while nanoribbons of type II are proposed for the Ggly(C_{10})$_2$ dodecane sample.

Also the structural properties of the quadruplexes forming in the presence of KPi depend on the considered derivative. Indeed, the less soluble (and less polar) G(C_{18}) gives rise to long, polydisperse quadruplexes, while short (and rather monodisperse) quadruplexes are formed by the other LipoGs. In particular, stacking ability appears to follow in dodecane the same order already observed in cyclohexane[47], *i.e.*, dG(C_{10})$_2$ $\simeq$ Ggly(C_{10})$_2$ < G(C_{18}): since a comparable average potassium hole occupancy has been detected for all the investigated systems (around 70%), additional stabilization terms may be related to the global LipoG molecular shape. Indeed, G(C_{18}) is flat, Ggly(C_{10})$_2$ is a little less planar and dG(C_{10})$_2$ is almost bent.

With respect to the behaviour observed in cyclohexane, one

main difference should be underlined: in dodecane, LipoG aggregates show a strong tendency to (laterally) interact. Bragg peaks (indicating the formation of columnar phases) and intense correlation bands have been in fact detected in several samples. In the absence of KPi, lyotropic behaviour appears when ribbons are *infinite* in length (in the case of Ggly$(C_{10})_2$, ribbons more than 200 nm long are present at the transition to isotropic phase), but in any case interparticle interactions are rather evident. ~~Noticeable is the fact that a structure factor based on hard-sphere interaction (e.g., excluded volume effect) can be successfully used to predict the pronounced interaction peaks.~~ In the presence of K^+, the appearance of ordered lyotropic phases (for continuity reasons indexed as *H* and *R*, for Gace(C_{10}) and Ggly$(C_{10})_2$, respectively) is probably caused by a low aggregation number, *i.e.*, when the quadruplexes are short, so that the particle number density is rather large. Indeed, heating induces a direct transition to the isotropic phase: on the basis of the approach developed by Taylor and Herzfeld[64], a stable nematic (or cholesteric) phase intervening between the hexagonal and isotropic phases can be found in columnar lyotropic systems only when finite rigid aggregates are on average sufficiently elongated.

In summary, the presented SAXS analysis gives a description of the different LipoG architectures occurring in hydrocarbon solvents, in the presence and in the absence of potassium ion. The quantitative estimate of G-ribbon flexibility and thermal stability, as well as the determination of G-quadruplex structural features, including ion hole occupancy, provide final insights into the relationship between LipoG organization at molecular and supramolecular level. Such information is clearly unavoidable for the design and development of new applications based on these biomaterials.

Acknowledgement

This study began several years ago, together with Piero Spada (Università di Bologna), who passed away in Bologna, on February 4th, 2013: we are indebted to Piero for all the skills, enthusiasm, friendship and energy he has shown in every moment of our long collaboration. We will miss him.

Notes and references

1 J.-M. Lehn, Angew. Chem. Int. Ed. Engl., 1988, **27**, 89–112.
2 V. Percec, A. E. Dulcey, M. Peterca, M. Ilies, S. Nummelin, M. J. Sienkowska and P. A. Heiney, Proc. Natl Acad. Sci. USA, 2006, **103**, 2518–23.
3 J. W. Shim, Q. Tan and L.-Q. Gu, Nucleic Acids Res., 2009, **37**, 972–982.
4 T. Aida, E. W. Meijer and S. I. Stupp, Science, 2012, **335**, 813–817.
5 L. Ruiz, P. V. Achen, T. D. Lazzara, T. Xu and S. Keten, Nanotechnology, 2013, **24**, 195103 (11 pp).
6 A. Zhang and C. M. Lieber, Chem. Rev., 2016, **116**, 215–257.
7 F. Pu, J. Ren and X. Qu, Chem. Soc. Rev., 2018, **47**, 1285.
8 L. Stefan and D. Monchaud, Nature Reviews Chemistry, 2019.
9 F. Aparicio, M. J. Mayoral, C. Montoro-García and D. González-Rodríguez, Chem. Commun., 2019, **55**, 7277.
10 M. Liu, G. Ouyang, D. Niu and Y. Sang, Org. Chem. Front., 2018, **5**, 2885.
11 M. Gellert, M. N. Lipsett and D. R.Davies, Proc. Natl. Acad. Sci. U.S.A., 1962, **48**, 2013–2018.
12 S. Arnott, R. Chandrasekaran and C. M. Marttila, Biochem. J., 1974, **141**, 537 – 543.
13 C. Detellier and P. Laslo, J. Am. Chem. Soc., 1980, **102**, 1135–1141.
14 P. Mariani, C. Mazabard, A. Garbesi and G. Spada, J. Am. Chem. Soc., 1989, **111**, 6369–6373.
15 G. Gottarelli, G. P. Spada and A. Garbesi, in Comprehensive Supramolecular Chemistry, ed. J.-M. Lehn, J. L. Atwood, D. D. MacNicol, J. A. D. Davies, F. Vögtle, J.-P. Sauvage and M. W. Hosseini, Pergamon Press, Oxford, 1996, vol. 9, pp. 483 – 506.
16 L. Spindler, I. Drevensek-Olenik, M. Copic and P. Mariani, Mol. Cryst. Liq. Cryst., 2003, **395**, 317–323.
17 L. Spindler, F. Federiconi, P. Mariani, I. Drevensek-Olenik, M. Copic, M. Tomic and A. Jamnik, Mol. Cryst. Liq. Cryst., 2005, **435**, 1/[661]–12/[672].
18 J. T. Davis, Angw. Chem. Int. Ed., 2004, **43**, 668–698.
19 J. Dash, A. J. Patil, R. N. Das, F. L. Dowdall and S. Mann, Soft Matter, 2011, **7**, 8120–8126.
20 N. Borbone, J. Amato, G. Oliviero, V. D'Atri, V. Gabelica, E. D. Pauw, G. Piccialli and L. Mayol, Nucl. Acids Res., 2011, **39**, 7848–7857.
21 E. Fadaei, M. Martín-Arroyo, M. Tafazzoli and D. González-Rodríguez, Org. Lett., 2017, **19**, 460.
22 Y. He, Y. Zhang, L. Wojtas, N. G. Akhmedov, D. Thai, H. Wang, X. Li, H. Guo and X. Shi, Chem. Sci., 2019, **10**, 4192.
23 J. T. Davis and G. P. Spada, Chem. Soc. Rev., 2007, **36**, 296–313.
24 S. Lena, S. Masiero, S. Pieraccini and G. P. Spada, Chem. Eur. J., 2009, **15**, 7792.
25 S. Masiero, L. Gramigna, P. Neviani, R. C. Perone, S. Pieraccini and G. P. Spada, I.RE.BI.C., 2011, **49**, 3657–3660.
26 M. E. Garah, R. C. Perone, A. S. Bonilla, S. Haar, M. Campitiello, R. Gutierrez, G. Cuniberti, S. Masiero, A. Ciesielski and P. Samorì, Chem. Commun., 2015, **51**, 11677.
27 G. Paragi and C. F. Guerra, Chem. Eur. J., 2016, **23**, 3042–3050.
28 W. Li, J. Jin, X. Liu and L. Wang, Langmuir, 2018, **34**, 8092.
29 G. Gottarelli, S. Masiero and G. P. Spada, J. Chem. Soc., Chem. Commun., 1995, **24**, 2555 – 2557.
30 A. Marlow, E. Mezzina, S. Masiero, G. P. Spada, J. T. Davis and G. Gottarelli, J. Org. Chem., 1999, **64**, 5116.
31 E. Mezzina, P. Mariani, R. Itri, S. Masiero, S. Pieraccini, G. P. Spada, F. Spinozzi, J. T. Davis and G. Gottarelli, Chem.-Eur. J., 2001, **7**, 388.
32 G. N. M. Reddy, A. Huqi, D. Iuga, S. Sakurai, A. Marsh, J. T. Davis, S. Masiero and S. P. Brown, Chem. Eur. J., 2017, **23**, 2315 – 2322.
33 G. Gottarelli, S. Masiero, E. Mezzina, G. P. Spada, P. Mariani and M. Recanatini, Helv. Chim. Acta, 1998, **81**, 2078.
34 G. Gottarelli, S. Masiero, E. Mezzina, S. Pieraccini, G. P. Spada and P. Mariani, Liq. Cryst., 1999, **26**, 965.
35 C. E. Hughes, G. N. M. Reddy, S. Masiero, S. P. Brown, P. A. Williams and K. D. M. Harris, Chem. Sci., 2017, **8**, 3971–3979.
36 J. Dash and P. Saha, Org. Biomol. Chem., 2016, **14**, 2157–2163.
37 A. Switalska, A. Dembska, A. Fedoruk-Wyszomirska and B. Juskowiak, Sensors (Switzerland), 2018, **18**, 2201.
38 G. Maruccio, P. Visconti, V. Arima, S. D'Amico, A. Biasco, E. D'Amone, R. Cingolani and R. Rinaldi, Nano Letters, 2003, **3**, 479–483.
39 X. Wang, L. Zhou, H. Wang, Q. Luo, J. Xu and J. Liu, Journal of Colloid and Interface Science, 2011, **353**, 412–419.
40 C. Arnal-Hérault, A. Banu, M. Barboiu, M. Michau and A. van der Lee, Angew. Chem. Int. Ed., 2007, **46**, 4268–4272.
41 S. Mihai, J. Dauthier, Y. L. Duc, A. E. Mansouri, A. Mehdi and M. Barboiu, Eur. J. Inorg. Chem., 2012, 5299–5304.
42 I. Yoshikawa, J. Li, Y. Sakata and K. Araki, Angew. Chem. Int. Ed., 2004, **43**, 100 – 103.
43 Y.-F. Gao, Y.-J. Huang, S.-Y. Xu, W.-J. Ouyang and Y.-B. Jiang, Langmuir, 2011,

27, 2958–2964.

44 C. Arnal-Hérault, A. Pasc, M. Michau, D. Cot, E. Petit and M. Barboiu, Angew. Chem. Int. Ed., 2007, **46**, 8409 –8413.

45 I. Yoshikawa, J. Sawayama and K. Araki, Angew. Chem. Int. Ed., 2008, **47**, 1038 –1041.

46 B. Roy, A. Depaix, C. Périgaud and S. Peyrottes, Chem. Rev., 2016, **116**, 7854–7897.

47 A. Gonnelli, M. Ortore, E. Baldassarri, S. Funari, S. Pieraccini, R. C. Perone, G. P. Spada and P. Mariani, J. Phys. Chem. B, 2013, **117**, 1095 âĹŠ1103.

48 T. Giorgi, F. Grepioni, I. Manet, P. Mariani, S. Masiero, E. Mezzina, S. Pieraccini, L. Saturni, G. P. Spada and G. Gottarelli, Chem.-Eur. J., 2002, **8**, 2143–2152.

49 L. R. S. Barbosa, M. G. Ortore, F. Spinozzi, P. Mariani, S. Bernstorff and R. Itri, Biophys. Journal, 2010, **98**, 147–157.

50 A. Guinier and G. Fournet, Small angle scattering of X-ray, Wiley, New York, 1955.

51 F. Spinozzi, C. Ferrero, M. G. Ortore, A. Antolinos and P. Mariani, Journal of Applied Crystallography, 2014, **47**, 1132–1139.

52 C. D. Putnam, M. Hammel, G. L. Hura and J. A. Tainer, Quarterly Reviews of Biophysics, 2007, **40**, 191–285.

53 P. Mariani, F. Spinozzi, F. Federiconi, H. Amenitsch, L. Spindler and I. Drevensek-Olenik, J. Phys. Chem. B, 2009, **113**, 7934–7944.

54 C. L. P. Oliveira, M. A. Behrens, J. S. Pedersen, K. Erlacher, D. Otzen and J. S. Pedersen, J. Mol. Biol., 2009, **387**, 147–161.

55 M. G. Ortore, P. Mariani, F. Carsughi, S. Cinelli, G. Onori, J. Teixeira and F. Spinozzi, Journal of Chemical Physics, 2011, **135**, 245103.

56 G. V. Schulz, Z. Phys. Chem., 1935, **43**, 25.

57 M. Kotlarchyk and S.-H. Chen, J. Chem. Phys., 1983, **79**, 2461–2469.

58 J. S. Pedersen and P. Schurtenberger, Journal of Applied Crystallography, 1996, **29**, 646–661.

59 S. Pieraccini, G. Gottarelli, P. Mariani, S. Masiero, L. Saturni and G. P. Spada, Chirality, 2001, **13**, 7–12.

60 S. Lena, G. Brancolini, G. Gottarelli, P. Mariani, S. Masiero, A. Venturini, V. Palermo, O. Pandoli, S. Pieraccini, P. Samorí and G. P. Spada, Chem. Eur. J., 2007, **13**, 3757–3764.

61 G. Gottarelli, S. Masiero, E. Mezzina, S. Pieraccini, J. Rabe, P. Samori and G. P. Spada, Chem.-Eur. J., 2000, **6**, 3242.

62 S. Lena, M. A. Cremonini, F. Federiconi, G. Gottarelli, C. Graziano, L. Laghi, P. Mariani, S. Masiero, S. Pieraccini and G. P. Spada, Chem. Eur. J., 2007, **13**, 3441–3449.

63 F. Federiconi, P. Ausili, G. Fragneto, C. Ferrero and P. Mariani, J. Phys. Chem, 2005, **109**, 11037–11045.

64 M. Taylor and J. Herzfeld, J. Phys. Condens. Matter, 1993, **5**, 2651–2678.